Constructing artificial respiratory chain in polymer compartments: Insights into the interplay between bo_3 oxidase and the membrane

Nika Marušič[a,1], Lado Otrin[b,1], Ziliang Zhao[c,1], Rafael B. Lira[c,1,2], Fotis L. Kyrilis[d,e], Farzad Hamdi (فرزاد حمدی)[d,e], Panagiotis L. Kastritis[d,e], Tanja Vidaković-Koch[b,3], Ivan Ivanov[a,3], Kai Sundmacher[a], and Rumiana Dimova[c]

[a]Process Systems Engineering, Max Planck Institute for Dynamics of Complex Technical Systems, 39106 Magdeburg, Germany; [b]Electrochemical Energy Conversion, Max Planck Institute for Dynamics of Complex Technical Systems, 39106 Magdeburg, Germany; [c]Department of Theory and Bio-Systems, Max Planck Institute of Colloids and Interfaces, 14424 Potsdam, Germany; [d]Interdisciplinary Research Center HALOmem, Martin Luther University Halle-Wittenberg, 06120 Halle/Saale, Germany; and [e]Institute of Biochemistry and Biotechnology, Martin Luther University Halle-Wittenberg, 06120 Halle/Saale, Germany

Edited by Michael L. Klein, Temple University, Philadelphia, PA, and approved May 14, 2020 (received for review November 5, 2019)

Cytochrome bo_3 ubiquinol oxidase is a transmembrane protein, which oxidizes ubiquinone and reduces oxygen, while pumping protons. Apart from its combination with F_1F_o-ATPase to assemble a minimal ATP regeneration module, the utility of the proton pump can be extended to other applications in the context of synthetic cells such as transport, signaling, and control of enzymatic reactions. In parallel, polymers have been speculated to be phospholipid mimics with respect to their ability to self-assemble in compartments with increased stability. However, their usability as interfaces for complex membrane proteins has remained questionable. In the present work, we optimized a fusion/electroformation approach to reconstitute bo_3 oxidase in giant unilamellar vesicles made of PDMS-*g*-PEO and/or phosphatidylcholine (PC). This enabled optical access, while microfluidic trapping allowed for online analysis of individual vesicles. The tight polymer membranes and the inward oriented enzyme caused 1 pH unit difference in 30 min, with an initial rate of 0.35 pH·min^{-1}. To understand the interplay in these composite systems, we studied the relevant mechanical and rheological membrane properties. Remarkably, the proton permeability of polymer/lipid hybrids decreased after protein insertion, while the latter also led to a 20% increase of the polymer diffusion coefficient in polymersomes. In addition, PDMS-*g*-PEO increased the activity lifetime and the resistance to free radicals. These advantageous properties may open diverse applications, ranging from cell-free biotechnology to biomedicine. Furthermore, the presented study serves as a comprehensive road map for studying the interactions between membrane proteins and synthetic membranes, which will be fundamental for the successful engineering of such hybrid systems.

GUV | polymersome | membrane protein | proton permeability | microfluidics

Synthetic biology is an umbrella term that exemplifies the recent paradigm shift in biology from a merely descriptive science to a powerful toolbox for manipulation and creation, analogous to synthetic chemistry. This concept has evolved in parallel with the increasing understanding of processes and underlying mechanisms in nature, and can be divided into two complementary approaches: top-down and bottom-up. The latter involves a stepwise integration of molecules to functional modules and further to minimal systems, whereby the hierarchical nomenclature (e.g., parts/modules/systems) is still used inconsistently among laboratories. While the studies of natural building blocks and their variable assemblies can be labeled as an evolved form of traditional in vitro experiments, the striving for understanding in the bottom-up approach is augmented by a creative aspect toward mimicking life processes in their entirety, alongside expanding and surpassing the natural. In this regard, the enrichment of the library of building blocks with synthetic alternatives (in the conventional semantics of chemically synthetic) could improve existing functionalities or introduce new ones (1). This incentive holds also in the case of cell membranes, where the scaffold phospholipids can be replaced with other amphiphilic molecules like synthetic polymers or blended with them in hybrid systems into a form of chemical prosthetics (2). Polymer vesicles (polymersomes) have a similar structure to liposomes and result from the self-assembly of polymers into monolayers (graft and triblock copolymers) or bilayers (diblock copolymers) (3). Polymersomes have been mainly used in the context of drug delivery (4, 5) including showcases like stimuli-responsive release (6) and cell targeting (7). The covalent bonds in polymers are generally more difficult to break than the ester

Significance

Analogous to phospholipids, some polymers assemble into vesicles and can mimic cellular membranes. Apart from enabling compartmentalization in the context of artificial cells, amphiphiles may serve as interface for proteins. However, complex transmembrane proteins were reconstituted in polymers with limited success so far. We functionally integrated the proton pump bo_3 oxidase (part of the bacterial respiratory chain) in synthetic membranes made of PDMS-*g*-PEO and demonstrated lumen acidification. We provided mechanistic insights into the interplay between the protein and the (semi) synthetic membrane by measuring bending rigidity, lateral diffusion and disorder, proton permeability, and protein partitioning. Polymer and hybrid membranes displayed favorable properties for the construction of artificial cells such as membrane rearrangement, enhanced stability and fluidity, while keeping the compartments proton-tight.

Author contributions: N.M., L.O., and I.I. designed research; N.M., L.O., Z.Z., R.B.L., F.L.K., and F.H. performed research; N.M., L.O., Z.Z., R.B.L., P.L.K., T.V.-K., I.I., K.S., and R.D. analyzed data; and N.M., L.O., and I.I. wrote the paper.

The authors declare no competing interest.

This article is a PNAS Direct Submission.

[1]N.M., L.O., Z.Z., and R.B.L. contributed equally to this work.

[2]Present address: Moleculaire Biofysica, Zernike Instituut, Rijksuniversiteit Groningen, 9747AG Groningen, The Netherlands.

[3]To whom correspondence may be addressed. Email: vidakovic@mpi-magdeburg.mpg.de or ivanov@mpi-magdeburg.mpg.de.

This article contains supporting information online at https://www.pnas.org/lookup/suppl/doi:10.1073/pnas.1919306117/-/DCSupplemental.

First published June 17, 2020.

bonds in phospholipids and degradation of repeating units would have a lower impact on the overall stability (3). In addition to chemical stability (8, 9), synthetic polymers offer increased resistance against aggregation (8, 10), broader chemical versatility (3), and increased tunability (11, 12). It is also possible to modify the size and morphology of the compartments by changing the hydrophilic/hydrophobic ratio (8, 13) or to functionalize the surface, e.g., for adhesion (14).

Amphiphilic assemblies serve another key role beyond compartmentalization; they act as interfaces for interactions with peripheral membrane proteins (MPs) and accommodate integral MPs. The latter take part in essential cellular processes such as selective transport and energy conversion, e.g., oxidative phosphorylation, in which electron transport chain (ETC) proteins pump protons across the membrane and the resulting proton-motive force (PMF) drives the synthesis of adenosine triphosphate (ATP). High PMF and reduced ETC have been linked to increased production of reactive oxygen species (ROS) in mitochondria (15, 16). ROS can induce peroxidation of lipids (unsaturated fatty acids) or cleave ester bonds and thus disrupt the bilayer arrangement, which may in turn inactivate MPs and increase the permeability (17, 18). With respect to this, partially or completely replacing the lipids with synthetic polymers, which are less prone to oxidation and hydrolysis, would increase the overall system stability.

For reconstitution of the energy machinery, it is crucial that the compartments have limited proton permeability in order to sustain a gradient. In addition, they have to offer a suitable environment for MPs, i.e., fluid and flexible membrane and thickness in the natural range (to avoid size mismatches, which may compromise protein folding). Until now, various MPs of the respiratory and photosynthetic ETC have been reconstituted in phospholipid microcompartments: bacteriorhodopsin (bR) (19), photosynthetic reaction center (RC) (20), bo_3 oxidase (21), and F_1F_o-ATPase (21, 22). On the other hand, MP reconstitution in polymer membranes is still rare and usually limited to nanosized compartments and less pretentious porins and channels (reviewed in ref. 23). In most cases, block copolymer membranes are too thick (2- to 10-fold thicker than the lipid bilayer), viscous, and rigid for the functional insertion of large and complex MPs (23–25). While in some cases the functional reconstitution was transparently demonstrated [proteorhodopsin in PMOXA-PDMS-PMOXA (26)], for other attempts the protein functionality may require further confirmation (27, 28).

Recently, we coreconstituted functional ubiquinol bo_3 oxidase and F_1F_o-ATPase in PDMS-*g*-PEO polymer and hybrid large unilamellar vesicles (LUVs) (29). Thereby, we observed completely retained activity of the four-subunit heme copper oxidase from *Escherichia coli* [144 kDa (30)], which catalyzes the reduction of dioxygen to water, coupling the redox energy to proton translocation through the membrane (31). Provided that historically other polymers have not been as suitable for complex MPs, it appeared important to elucidate the mechanical characteristics of a successful platform, apart from the matching thickness. It is known that reconstituted MPs exert forces on membranes and change their mechanical properties. For instance, decrease in membrane stiffness (22, 32–34), membrane fluidity (35, 36), and increase in passive proton permeability (37) have been reported, whereby the latter is a decisive parameter for the cellular energetics. However, whether and to what extent the reconstituted MPs change the mechanical properties of polymer and hybrid membranes is still unknown. It is also largely unexplored how the graft copolymer affects the functional durability of such a system and whether it can improve the stability against chemicals.

To address these questions, we investigated the interactions between synthetic [polydimethylsiloxane-graft-poly(ethylene oxide) (PDMS-*g*-PEO) (for chemical structure, see *SI Appendix*, section S1.1 and Scheme S1)] and hybrid (PDMS-*g*-PEO/soy PC) membranes with bo_3 oxidase. First, we monitored the activity of the proton pump in these membranes over time and in the presence of ROS. To form compartments of tangible size and compatible with optical methods, i.e., in the micrometer range, we used electroformation from nanosized prereconstituted vesicles (19) and optimized the procedure for the particular MP and amphiphiles. In addition, we demonstrated the versatility of the protocol by applying it for F_1F_o-ATPase, a MP with different size, hydrophobicity, and symmetry. Next, we analyzed the protein distribution and characterized its influence on the bending rigidity, membrane fluidity, and proton permeability, whereby in all cases the synthetic polymer membranes were benchmarked against the natural phospholipid analog. Microfluidic devices for hydrodynamic trapping (38) turned out particularly useful for permeability and pumping experiments, allowing control over the solution exchange and facilitating optical observations. Finally, the mechanistic understanding of the observed behavior was supported by cryo-TEM imaging, membrane order analysis, and protein partitioning analysis via fluorescence resonance energy transfer (FRET). Altogether, the scale-up of the functionalized compartments to the micrometer range enabled real-time visualization and detailed characterization of the interplay in the minimal respiratory chain module, while opening possibilities for the design of complex systems.

Results and Discussion

1. PDMS-*g*-PEO Extends the Activity Lifetime of bo_3 Oxidase and Prevents Enzyme Delipidation and Deactivation by ROS. Reconstituted complex MPs are known to drastically lose activity with time, whereby the rate of the loss depends on the protein type and the environment. While block copolymers have been shown to increase the functional stability (24), graft copolymers are still largely unexplored in this context. In addition to the shelf life of individual MPs, collateral damage caused by other enzymes may present an issue in more complex systems, e.g., oxidative stress in ETC assemblies. To test whether PDMS-*g*-PEO can enhance the stability, we applied detergent-mediated reconstitution by slightly modifying our previous protocol (29) and inserted bo_3 oxidase in ∼100-nm nanocompartments made of soy PC, PDMS-*g*-PEO/soy PC (70:30 molar ratio) and PDMS-*g*-PEO at a constant lipid/polymer-to-protein molar ratio of 9,550:1. We intermittently measured protein activity in all three systems over 13 d and in addition exposed them to oxidative stress by incubation with ascorbyl free radicals following established protocols (39, 40). The assessment was based on oxygen reduction, which is coupled to proton pumping (31, 41). Oxygen consumption was measured using a Clark-type electrode (*SI Appendix*, section S3.2). The protein was activated with the electron shuttle ubiquinone 1 (Q_1) and DTT under nonlimiting concentration of the sacrificial electron donor (Fig. 1 *A*, *Inset*).

Interestingly, when keeping the same lipid/polymer-to-protein molar ratio, bo_3 oxidase had the highest activity in hybrids, while activity in polymersomes and liposomes was virtually the same (day 1, *SI Appendix*, section S10 and Fig. S1*A*). The superior properties of hybrids were reflected in stability tests as well. On day 2, they retained 90% of the initial activity, while liposomes and polymersomes decreased to 63% and 69%, respectively (Fig. 1*A*). Similar relation was present toward the end of the measurements. On day 11, the activity of liposomes decreased to 4%, while hybrids and polymersomes retained 25% and 15%, respectively (*SI Appendix*, section S10 and Fig. S1*A*). Despite the scattering of the data, the qualitative trend (hybrids > polymersomes > liposomes) was maintained throughout the test. This was clearly evident also from the respective time constants of exponential decay (4.1 > 1.5 > 0.7), which reflected the days until the vesicles lost roughly one-third of their initial activities, even though the fit of liposome data might have led to some underestimation of the stability (*SI Appendix*, section S10

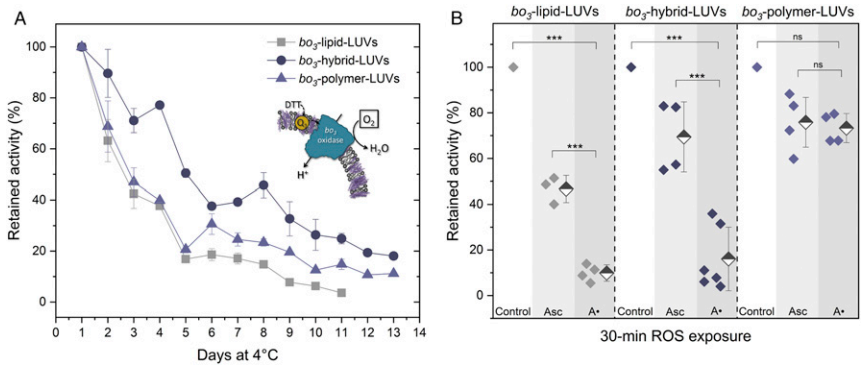

Fig. 1. (*A*) Activity of bo_3 oxidase reconstituted in LUVs over time at 4 °C, determined via oxygen consumption and measured every 24 h (each symbol represents the average of two to three repeats with SD). (*B*) Activity retention of bo_3 oxidase after incubation with ascorbate (Asc) and ascorbyl free radical (A•) for 30 min. For 100% (control) activity of untreated bo_3-LUVs was taken (two to three repeats). Individual data are shown as filled diamonds; average values are shown as half-filled diamonds and SD. ns, not significant for $P > 0.05$; ***$P \leq 0.001$.

and Fig. S1*B*). The loss of activity was ascribed to the protein due to the similar behavior in micelles, but the detailed mechanism of preservation should be clarified in a more detailed study. It is worth noting that the blending with graft copolymer resulted in a similar improvement (~20%) of the stability in comparison to pure lipids as in the case of PBd-*b*-PEO/POPC (75:25) hybrid vesicles after 1 wk (24). As previously emphasized (42), hybrids hold a great promise for the reconstitution of MPs, whereby the enhanced durability, stability, and shelf life will be essential for application. PDMS-*g*-PEO/PC hybrids in particular may not only have a stabilizing effect but also increase the activity (presumably via higher reconstitution efficiency, yet to be determined). On the other hand, PDMS-*g*-PEO seems to be the only polymer so far, which enables fully retained bo_3 oxidase activity in addition to stabilization.

The incubation with ascorbate and ascorbyl radicals did not cause a change in the size distribution (*SI Appendix*, section S11.1 and Table S1), but it decreased enzyme activity. However, PDMS-*g*-PEO shielded the proteins against oxidative stress; after 30 min of exposure to radicals, polymersomes retained 73 ± 6% activity, while liposomes, only 10 ± 4% (Fig. 1*B*). In addition, it should be noted that the activity decrease in polymersomes was statistically nonsignificant. The chemical resistance of the graft copolymer substantiates its suitability to accommodate complete ETC and to counteract the detrimental influence of ROS (produced by Complex I in particular). The activity loss upon ROS exposure can be caused either by a direct attack to the reconstituted MP or by indirect deactivation via membrane disruption and enzyme delipidation. Since the vesicle size did not change, we sought for subtle changes associated with surface modifications and/or compromised tightness. Therefore, we measured the surface charge of the vesicles without reconstituted bo_3 oxidase and tested the leakage of encapsulated carboxyfluorescein (CF) by its dequenching (43). The different conditions did not significantly alter the zeta potential results within the instrument accuracy (*SI Appendix*, section S11.2 and Fig. S2). On the other hand, while liposomes were permeabilized upon radical exposure (*SI Appendix*, section S11.3 and Figs. S3*A*, S4, and S5), no leakage was detected in polymersomes and hybrids (*SI Appendix*, section S11.3 and Fig. S3 *B* and *C*), indicating absence of membrane defects. In addition, we inspected protein-functionalized vesicles after oxidative treatment by cryogenic transmission electron microscopy (cryo-TEM). A portion of the liposomes exhibited bilayer defects manifested as either visible pores or irregular surface (*SI Appendix*, section S18.2 and Fig. S33). Such membrane disruptions by ROS likely lead to delipidation of bo_3 oxidase and consequently to enzyme aggregation and deactivation (complete loss of activity in the absence of stabilizing amphiphiles is shown in *SI Appendix*, section S12.4 and Fig. S12). On the contrary, no difference between the cryo-TEM images of ROS-treated and untreated samples was observed in both hybrids and polymersomes.

Finally, we tested the effect of ROS on the enzyme alone (i.e., bo_3 oxidase, which was not reconstituted in a membrane but stabilized in detergent micelles) and no loss of activity was observed. In fact, the oxygen consumption slightly increased, presumably due to direct reduction of hemes by ascorbate (25.5 ± 3.4 vs. 20.8 ± 3.5 $\mu M \cdot min^{-1}$). These observations further emphasize the importance of a stable scaffold even when the integrated MPs are otherwise resistant to ROS. Furthermore, the structural integrity of the membrane is imperative for reaction compartmentalization or cargo delivery.

2. Scale-Up from Nano to Micro: Access to Single Vesicles in Controlled Environment.

2.1. Preparation of bo_3-GUVs from prereconstituted lipid, hybrid, and polymer LUVs. The reconstitution of complex MPs into GUVs (44) is not a straightforward task due to the incompatibility of enzymes with organic solvents used in the traditional electroformation procedure (45) or in phase-transfer methods (46). Previously, detergent-stabilized bo_3 oxidase has been inserted into preformed lipid GUVs by subsequent dilution of the detergent, which resulted in a protein density of ~30 proteins·μm^{-2} (47). However, this approach turned out to be inefficient particularly for the polymer membranes because it substantially decreased the protein activity. In addition, remaining traces of detergent can change the membrane properties and increase the proton permeability (37, 48). We previously screened different mild detergents and optimized their concentrations and subsequent removal to obtain functional proteins in different types of LUVs (29). Seeking to reflect this performance on the GUV scale (e.g., retain a favorable orientation), we used the same reconstitution protocols and afterward converted the proteoLUVs into proteoGUVs via electroformation from a partially dried LUV film (19) (the three main steps are presented in *SI Appendix*, section S4.2 and Scheme S4), whereby we note that the dehydration step required precise control.

For the subsequent tests, it was important that the GUVs were sufficiently large (minimum diameter of 10 to 20 μm or preferably larger). Therefore, we optimized the protocol to obtain vesicles in the desired size range (typical distributions in *SI Appendix*, section 12.3 and Fig. S9). To avoid phase separation in the hybrid GUV membranes (29) and potential budding (49), we used a ratio of 70 mol% PDMS-*g*-PEO to 30 mol% soy PC. This ensured a homogenous distribution on the micrometer scale (*SI Appendix*, section S12.1 and Fig. S6). To prove the successful protein incorporation, we labeled bo_3 oxidase with ATTO 514 and analyzed its distribution in lipid, hybrid, and polymer GUVs by confocal microscopy (*SI Appendix*, section S12.2 and Fig. S8). No phase separation and aggregation were observed (Fig. 2*A*), suggesting uniform protein distribution.

We next probed whether the activity of bo_3 oxidase is retained after the scale-up to GUVs because a complete dehydration may have a deleterious effect on the activity of MPs (19). For this, we

relied on measurement of the oxygen reduction. The oxygen consumption of different bo_3-GUVs (see *SI Appendix*, section S12.3 for sample quality) and ∼100-nm bo_3-LUVs (*SI Appendix*, section S12.3 and Fig. S10) was determined from bulk samples. For results on enzymatic activity retention and homogeneity of the protein distribution, please see *SI Appendix*, section S12.4.

2.2. bo_3 oxidase acidifies synthetic microcompartments. Following the populational activity characterization of the bo_3-GUVs via oxygen consumption, we next probed the proton translocation on a single-vesicle level. Characterization of individual vesicles provides additional information, which could be overlooked and averaged in bulk tests due to vesicle rupture and size variance. Here, we were able to directly deduce the enzyme orientation by observing the net ΔpH upon chemical activation. Since it was previously shown that the orientation of a complex MP such as Ca^{2+}-ATPase is retained upon the fusion/electroformation approach (19), we focused solely on the novel system, namely bo_3 oxidase reconstituted in PDMS-*g*-PEO GUVs.

Similar observations were done only for bR (19, 50) and a RC (20) in conventional observation chambers. The downside of the latter setup is that the vesicles could move out of focus if not deliberately immobilized to the surface (which in turn can alter the membrane tension and local composition) and the external solution cannot be exchanged completely; instead, the samples are being diluted. While this effect is irrelevant for light-activated proton pumps, we preferred that oxygen and Q_1/DTT were supplied in a defined manner. For that purpose, we followed the luminal pH changes in a microfluidic device (*SI Appendix*, section S5.2), which contained multiple rectangular traps similar to those in ref. 38, with a gap size of about 5 μm between the posts forming the trap (*SI Appendix*, section S1.4 and Scheme S2). This enabled entrapment of multiple GUVs with diameters >10 μm and did not compromise their structural and functional integrity. The ΔpH was evaluated by encapsulation of the established ratiometric pH-sensitive dye pyranine (51, 52). Briefly, bo_3-GUVs were prepared in weakly buffered solution (100 mM sucrose, 1 mM Tris·HCl, pH 7.5) in the presence of 10 μM pyranine, then trapped and washed by flushing pyranine-free buffer in the microfluidic chip. Next, proton pumping was initiated by flushing in 40 μM Q_1 and 8 mM DTT (Fig. 2*C*). Ratiometric measurements are advantageous as they are virtually insensitive to differences in pyranine encapsulation and photobleaching.

The luminal pH decreased upon activation and the established ΔpH correlated with the increasing amount of bo_3 oxidase per vesicle, while the pH in protein-free polymersomes stayed fairly constant. bo_3-GUVs with a molar ratio of 9,540:1 polymer-to-protein acidified by nearly 0.3 pH units in the first 3 min and tripling the protein content (2,980:1) increased ΔpH to 0.5 in roughly the same time (Fig. 2*D*). After that, the pH in GUVs with higher protein loading continued to decrease at a much lower rate: ∼0.2 units over 25 min and overall ΔpH after 30 min exceeded 1 unit. The ΔpH and timescales for bo_3 oxidase in the synthetic membrane were comparable with light-induced proton pumping in lipid membranes. bR reconstituted in lipid GUVs was observed to lower the intravesicular pH by 0.8 pH units in 30 min (50), while RC was shown to cause an increase by ∼0.8 pH units in 15 min (20). The lipid-to-protein molar ratios of reconstituted bR (2,200 ± 700) and RC (2,200) were slightly higher than the polymer-to-protein molar ratio (2,980) used in this study. The similarity in performance is a good indicator for the viability and biocompatibility of the PDMS-*g*-PEO membranes toward complex MPs.

At higher protein loading, the increased pumping rate was sustained for about 3 min and was followed by more moderate decrease (individual trace in *SI Appendix*, section 13.2 and Fig. S16). The initial fast rate took more than a minute to fully develop, which we ascribed to partitioning of Q_1 into the membrane and diffusion to the enzyme [the latter is a rate-limiting step in the mitochondrial ETC (52)]. Interestingly, the rate did not decrease progressively but very sharply. Note that the traces are averaged and the scattering is due to the size variance. However, the high protein loading data were very reproducible; therefore, we could clearly identify a changing rate: 0.35 pH·min^{-1} and 0.64 × 10^{-2} pH·min^{-1}. Decrease of the pumping rate has been observed also in the case of bR-liposomes [reaching a steady state after about 3 min (53) or 5 to 6 min (19) of illumination], which was ascribed to a retroinhibition by the established ΔpH (back-pressure effect) (53).

The magnitude of the pH gradient directly depends on the type and amount of reconstituted MPs. While light-driven proton pumps, such as bR, provide the virtue of orthogonality with respect to the energy source, chemically driven pumps such as bo_3 oxidase have higher turnovers (300 to 341 s^{-1} vs. 37 to 50 s^{-1}) (1) and introduce additional means for coupling with metabolic reactions. With respect to the reconstitution of the energy machinery, the enzyme orientation in the membrane plays a pivotal role as well. The latter can be controlled by the type of detergent and the experimental conditions, but it is largely determined by the membrane. Prevailing

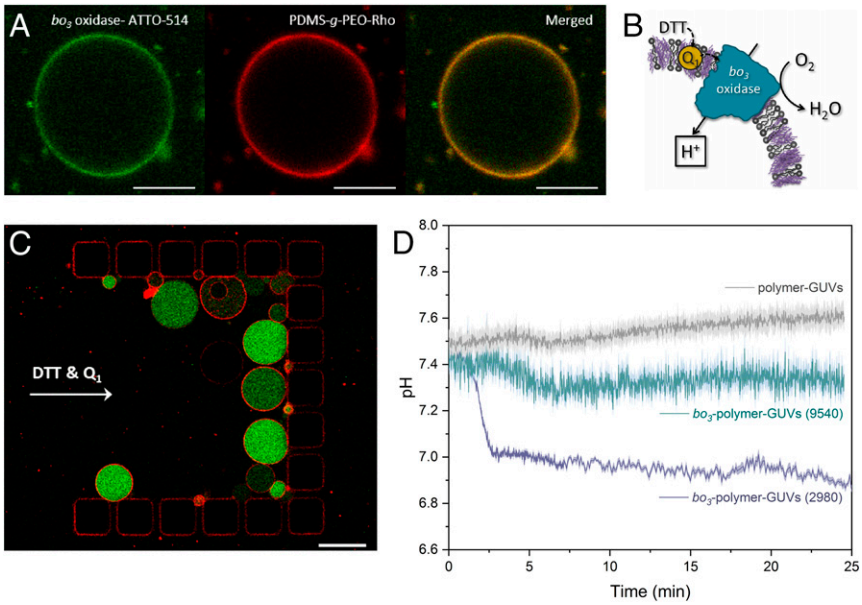

Fig. 2. (*A*) Successful insertion and homogenous distribution of bo_3 oxidase-ATTO 514 (green) in bo_3-polymer-GUVs. Polymer labeled with rhodamine (PDMS-*g*-PEO-Rho, red) was used to visualize the membrane. (Scale bar, 10 μm.) Distribution of bo_3 oxidase-ATTO 514 in hybrid and lipid GUVs is depicted in *SI Appendix*, section S12.2 and Fig. S8. (*B*) Scheme of activated bo_3 oxidase with correct orientation (inward pumping). (*C*) bo_3-polymer-GUVs (PDMS-*g*-PEO:bo_3 oxidase, 2,980:1 mol/mol) with encapsulated pH-sensitive pyranine (green) trapped in microfluidic chip. Membrane was stained with 0.05 mol% PDMS-*g*-PEO-Rho (red). (Scale bar, 50 μm.) (*D*) Intravesicular pH change for negative control (protein-free vesicles; gray trace), and two types of GUVs with different polymer-to-protein molar ratios; 2,980:1 (purple trace) and 9,540:1 (green trace) upon activation with DTT/Q_1 reached bo_3-polymer-GUVs trapped in the microfluidic chip. Each trace represents the mean of five to seven individual vesicles and their SD.

inward orientation of bo_3 oxidase was previously deduced in DOPC SUVs (54) and later on in PDMS-*g*-PEO LUVs (29) from the respiratory-driven ATP synthesis (possible only with favorable gradient direction). Here, we confirmed the utility of the reconstitution method and the synthetic membrane, alongside the scale-up procedure through direct visual observation of the pH change. In addition, it can be anticipated that even higher ΔpH could be established at the interface, where protons might accumulate before diffusing into the vesicle lumen. This has been postulated in phospholipid membranes at distances between bo_3 oxidase and F_1F_o-ATPase shorter than 80 nm, in which the lateral proton transfer along the surface was faster than equilibration with the bulk water (47). With respect to the synthetic interface, bo_3 oxidase has been previously reconstituted in PBd-*b*-PEO, but the protein was functional only in combination with POPC, i.e., in hybrid LUVs (42). The latter showed increased durability, but the random (symmetrical) orientation resulted in subtle pH changes (no data shown). The activity in the present study substantiates the choice of the graft copolymer for bo_3 oxidase and provides the potential to extend this synthetic platform to other complex MPs, beyond ETC enzymes.

3. PDMS-*g*-PEO and Hybrid Membranes Are Softer than Lipid Ones, and the Bending Rigidity Decreases upon Protein Insertion. The bending rigidity (κ) is an important membrane characteristic with implications on cellular mimics as it reflects the resistance to deformation (55), which vesicles may experience during division, fusion, or osmotic shock. Furthermore, there is a common notion that increased rigidity impedes the reconstitution and most importantly the activity of complex MPs. The bending rigidity of fluid lipid membranes is typically in the order of 10 to 20 k_BT (56), while polymersomes can exhibit various stiffness [up to 400 k_BT (3)], depending on the membrane thickness. Commonly used block polymersomes have usually higher rigidity, for example PEO-PBD [35 ± 6 k_BT (11)], but there are also block copolymers that form much softer membranes such as Pluronic L121 [PEO_5-PPO_{68}-PEO_5, ∼3 k_BT (11)]. To unveil how susceptible to bending are PDMS-*g*-PEO and hybrid membranes, we tracked the membrane fluctuations in GUVs by means of flickering spectroscopy (57) as described in ref. 58. To allow for visible membrane fluctuations, we exposed GUVs to gentle hypertonic conditions (*SI Appendix*, section S6.1). A large fraction of the lipid and polymer GUVs exhibited tubes and buds [possibly resulting from buffer asymmetry (59)] and these vesicles were not analyzed, while the hybrid GUVs appeared less tubulated. PDMS-*g*-PEO GUVs exhibited twice lower rigidity than soy PC (Fig. 3*A*). Rather than showing intermediate softening, hybrids exhibited lower bending rigidity than liposomes, comparable to that of pure polymersomes (i.e., 11.6 ± 2.4 k_BT), which indicates that this property is largely determined by the prevailing membrane component.

Previous studies report lipid membrane softening upon MP insertion in the case of Ca^{2+}-ATPase (33), while in other cases softening occurred only after protein activation: bR (32, 60, 61), Na^+/K^+-ATPase (34), and F_1F_o-ATPase (22) (summarized in *SI Appendix*, section S14 and Table S3). To check the influence of bo_3 oxidase on the lipid and graft copolymer membranes, we performed fluctuation analysis upon reconstitution. Polymer GUVs and bo_3-polymer-GUVs were on average tenser than protein-free and protein-functionalized hybrids and liposomes, which suppressed fluctuation. Therefore, further deflation was necessary (additional ∼5 min with open chamber to allow water evaporation). In addition, upon further deflation of the bo_3-polymer-GUVs, the excess area almost exclusively formed tubes instead of enhancing fluctuation, enabling only a narrow window for analysis. We speculate that the reason for this phenomenon was the protein-induced asymmetry, as it is known that transiently bound or constitutively inserted MPs can alter the spontaneous curvature (33) and cause invaginations or tubulations (62). bo_3 oxidase introduces slight asymmetry through its shape [predominantly hydrophobic truncated cone and small cytosolic fragment (63) (*SI Appendix*, section S19 and Fig. S41)]. Reconstitution of the proton pump caused membrane softening in all three types of membranes (20% for polymer, 26% for hybrid, and 30% for lipid membrane; Fig. 3*A* and *SI Appendix*, section S14 and Table S3). This indicates that the graft copolymer membrane responds to the inserted proton pump in the same manner as lipid membranes and no undesirable rigidification is taking place. Retention of the membrane softness after protein insertion is crucial for the reconstitution of additional MPs as well as for integration with other functional modules of artificial cells such as motility, division, and growth. Because it was previously demonstrated that nonactive integral MPs only slightly change the bending rigidity of lipid membranes, and to a considerable extent only when they were active (22, 33, 64), we expect a larger influence of pumping bo_3 oxidase (in presence of activators). In addition, we speculate that the asymmetry will be enhanced by the unidirectional proton pumping if the proteins have adopted a preferred orientation. However, the assessment of activated membranes was not feasible due to very short window available for analysis during which DTT was already oxidized.

The difference in bending rigidity arises not only from the chemistry of the constituents but also from the arrangement they adopt in those membranes. Cryo-TEM analysis indicated that the protein-free membrane thickness slightly increased with increasing amount of polymer: 4.40 ± 0.16 nm for lipid, 4.86 ± 0.17 nm for hybrid, and 5.25 ± 0.17 nm for polymer membrane. Furthermore, we observed distinct structural differences between all three types of membranes. Lipid LUVs had a bilayer structure with sharp outer boundaries, while polymer membranes appeared as fuzzy monolayers (Fig. 3*B*). Meanwhile, two populations of hybrid vesicles were observed: one-third resembled polymersomes, while lipid nanodomains of different sizes (discussed in more detail in section 5) were observed in the rest (two-thirds) of the hybrid LUVs.

4. Protein Insertion Increases the Fluidity of the Polymer Membrane. MPs can confer biological functionalities to synthetic membranes only when the former retain structural and functional integrity upon reconstitution. Key factors for this are the flexibility and fluidity of the membrane, which largely determine the lateral mobility of the protein (65, 66). In the case of bo_3 oxidase, it is also important that the ubiquinone shuttle can readily diffuse to the active sites of the enzyme. Commonly used block copolymer membranes have significantly lower fluidity compared to lipid membranes [e.g., diffusion coefficients of 0.22 ± 0.06 $\mu m^2 \cdot s^{-1}$ for PBd_{46}-*b*-PEO_{30} (67) vs. 10.0 ± 0.4 $\mu m^2 \cdot s^{-1}$ for DOPC (68)], which appears to be one of the reasons for the hindered functionality of MPs. Therefore, we checked whether PDMS-*g*-PEO provided similar fluidity to the natural environment. To this end, we determined the lateral diffusion of protein, polymer, and lipid by measuring the fluorescence recovery after photobleaching (FRAP). Lipid and polymer were labeled with rhodamine (Rho) and bo_3 oxidase with ATTO 514.

The soy PC membrane, used as a benchmark in this study, has a similar fluidity to the commonly used POPC and DOPC membranes (*SI Appendix*, section S15 and Table S4). In hybrids and polymersomes, the diffusion coefficients of the polymer dye decreased to approximately one-half and one-third of the diffusion coefficient of the lipid dye measured in natural membrane, respectively. Fluidity of the PDMS-*g*-PEO membrane was in line with previous reports for the same polymer (69) and in fact, similar to that of SOPC (3.8 ± 0.2 $\mu m^2 \cdot s^{-1}$) (70). The high fluidity of the graft copolymer can be partially attributed to the relatively low molecular weight of PDMS-*g*-PEO (molecular weight, 3,000 $g \cdot mol^{-1}$) and the PDMS backbone (71).

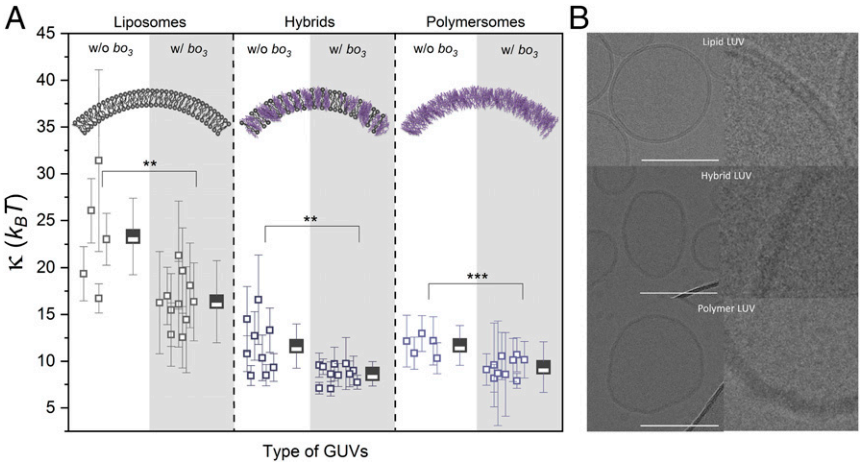

Fig. 3. (*A*) Bending rigidity (κ) for protein-free (w/o bo_3; white area) and protein-functionalized (w/ bo_3; gray area) liposomes, hybrids, and polymersomes. Each square represents a measurement on a single GUV and its SD (result of the fitting). Half-filled squares represent the average of all evaluated GUVs and the average SD. For statistical significance analysis, see *SI Appendix*, section S6.4. (*B*) From *Top* to *Bottom*: cryo-TEM micrographs of soy PC, PDMS-*g*-PEO/soy PC, and PDMS-*g*-PEO LUVs. (Scale bar, 100 nm; defocus, approximately −2 μm.) Additional images of all three types of vesicles can be found in *SI Appendix*, section S18. $^{**}P \leq 0.01$; $^{***}P \leq 0.001$.

Insertion of bo_3 oxidase led to a ∼20% decrease of the diffusion coefficients of the labeled lipids in liposomes and the labeled polymers in hybrids (Fig. 4*A* and *SI Appendix*, section S15 and Table S4), while the diffusion coefficients of labeled lipids in hybrids and polymersomes decreased by 32%. Similar decrease in fluidity upon reconstitution of the *E. coli* outer MPs FhuA, LamB, NanC, OmpA, and OmpF was demonstrated in POPE/POPG bilayers (35). The latter effect was explained by the less smooth surface and the presence of concave regions in the MPs that trapped phospholipids, resulting in overall steric hindrance, which scenario should apply in the present case as well. Interestingly, this phenomenon was not observed in the case of the polymer dye in polymer membranes. On the contrary, the diffusion coefficient increased by 23%. We attributed this to the partitioning of the enzyme into the intertwined PDMS chains, which loosened their assembly and increased the diffusion of the tagged polymer (discussed below). In contrast, the repositioning of lipid molecules in the lipid and hybrid membranes could compensate for the structural disorder, caused by the insertion of bo_3 oxidase. The lower mobility of labeled lipids (0.3 mol%) in polymersomes (Fig. 4*A*) supported such a repositioning around the protein. The diffusion coefficients of proteins and lipids are known to decrease linearly with increasing protein concentration (35, 36). However, an excessive decrease of the membrane fluidity could potentially hinder the conformational changes of MPs. Therefore, the preserved fluidity of polymer membranes upon protein reconstitution may prove valuable for applications, which require higher protein density.

In the case of lipid and hybrid membranes, the lateral diffusion of bo_3 oxidase was faster than the diffusion of lipid and polymer dye, while in pure polymer we observed the opposite. Altogether, the protein diffusion slowed down from liposomes to polymersomes, which was analogous to the trend for the fluidity of protein-free membranes. The superimposition of properties of natural and synthetic materials resulted in the intermediate values observed for hybrids. The diffusion coefficient of labeled bo_3 oxidase in soy PC ($9.9 \pm 1.3\ \mu m^2 \cdot s^{-1}$) was identical to the previously determined by fluorescence correlation spectroscopy in DOPC and similar to the diffusion coefficients of smaller MPs in POPC (*SI Appendix*, section S15 and Table S4). On the other hand, the protein diffusion in PDMS-*g*-PEO ($3.5 \pm 0.9\ \mu m^2 \cdot s^{-1}$) was at least two times higher than the diffusion of porins and channels in a triblock copolymer membrane. For instance, the diffusion coefficient of KcsA decreased nearly sevenfold upon transition from lipid to polymer ($PMOXA_7$-*b*-$PDMS_{49}$-*b*-$PMOXA_7$) environment (65), while for bo_3 oxidase in PDMS-*g*-PEO the decrease was less than threefold. We ascribed the favorable properties of the graft copolymer to the membrane thickness and the sufficient fluidity. In thicker membranes, the hydrophobic size mismatch between the membrane and the MP is more pronounced and the polymer molecules compress the MP stronger, which reduces its lateral mobility (65). In fact, the hydrophobic matching and slight compression of the PDMS-*g*-PEO membrane around the enzyme can be seen in cryo-TEM (see Fig. 8).

Since our overarching aim is the reconstitution of the entire ETC comprising several MPs, we checked whether the increase in polymer membrane fluidity upon protein insertion is bo_3 oxidase-specific or a general phenomenon. Toward this end, we labeled *E. coli* F_1F_o-ATPase with ATTO 620 and reconstituted it in hybrid and polymer GUVs by the same tailored fusion/electroformation protocol used for the proton pump, which demonstrated its utility for larger [F_1F_o-ATPase >500 kDa (72)] and highly asymmetric MPs (Fig. 4*B* and *SI Appendix*, section S15 and Figs. S19 and S20). Because of the lower reconstitution efficiency, which resulted in lower fluorescence signal, we were unable to obtain reliable data for the protein diffusion. Nevertheless, the analysis of the labeled lipids and polymers demonstrated that the loosening of PDMS-*g*-PEO after protein insertion is not protein specific: The diffusion of the polymer dye in polymersomes increased by 25% upon reconstitution of F_1F_o-ATPase (Fig. 4*A*).

Finally, we inspected the protein-induced loosening of the polymer membrane in more detail by analyzing the degree of disorder by a fluorescent probe in LUVs. Laurdan exhibits a red shift when set into more polar environment (presence of water in the membrane) (73), and the resulting generalized polarization (GP) values (for more details, see *SI Appendix*, section S6.3) range from +1 (most ordered membranes) to −1 (most disordered membranes) (74). Soy PC membranes exhibited similar order to DOPC membranes [GP of soy PC was -0.26 ± 0.01 vs. -0.24 ± 0.00 for DOPC (74)], while polymer membranes displayed significantly higher disorder or water content (about 50% lower GP values) (Fig. 5*B*). Meanwhile, intermediate GP values were determined for hybrid membranes. The reconstitution of bo_3 oxidase caused a slight decrease only in the case of PDMS-*g*-PEO, which was in line with the hypothesis of loosened polymer architecture.

5. Membrane Reorganization Reseals Hybrid Membranes after Protein Insertion. The passive proton permeability is arguably the most important membrane characteristic with respect to the reconstitution of proton pumps because it is fundamental for the establishment and sustainment of pH gradient. The insertion of bR has been shown to alter the tightness with respect to proton transport

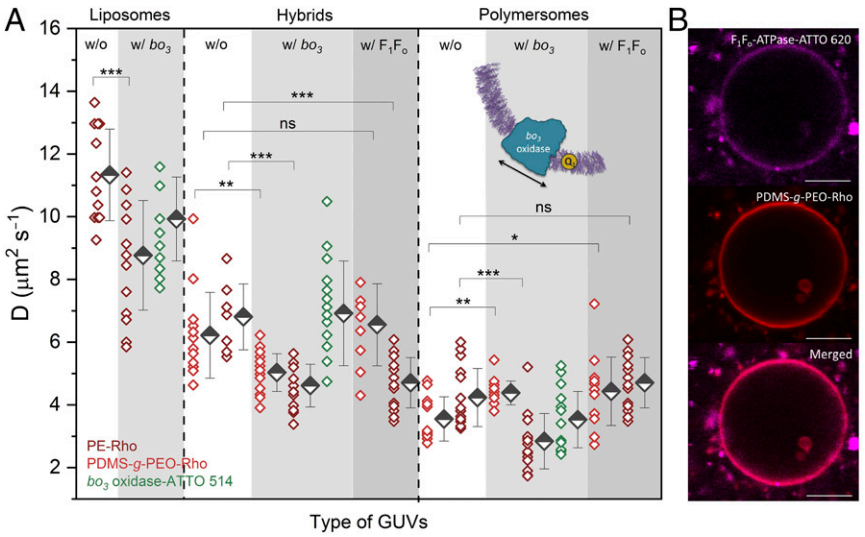

Fig. 4. (*A*) Diffusion coefficients for protein-free (w/o; white area) and protein-functionalized (w/ bo_3, light gray area; w/ F_1F_o, dark gray area) GUVs. Diffusion coefficients of lipid and polymer dyes are presented with red diamonds (PE-Rho, dark red; PDMS-*g*-PEO-Rho, light red); diffusion coefficients of bo_3 oxidase-ATTO 514 are presented with green diamonds. (*B*) Successful insertion of F_1F_o-ATPase-ATTO 620 (magenta) in F_1F_o-polymer-GUVs. Polymer dye PDMS-*g*-PEO-Rho (red) was used to visualize the membrane. (Scale bar, 10 μm.) Distribution of F_1F_o-ATPase-ATTO 620 in hybrid GUVs is depicted in *SI Appendix*, section S15 and Fig. S19. ns, not significant for $P > 0.05$; *$P \leq 0.05$; **$P \leq 0.01$; ***$P \leq 0.001$.

(37), but altogether, the systematic studies on the influence of MPs are scarce and to the best of our knowledge have never been done for synthetic membranes in particular. Therefore, we determined the passive proton permeability of the pristine and protein-functionalized membranes by direct monitoring of GUVs and supported the obtained results through experiments with ∼200-nm LUVs (*SI Appendix*, section S7.1–S7.3).

Thus far, the passive proton permeability of various membranes was predominantly measured in large vesicles (75–78). While these bulk LUV studies enable the measurements of large populations at once, liposome intactness is occasionally questionable, and the obtained values might not accurately depict the heterogeneity of the sample (79). In this regard, the convenience and the higher confidence of observations in the micrometer range could be potentially extended to account for individual attributes such as membrane curvature or compositional differences. Efforts in this direction have already been made: The permeability of lipid membranes with reconstituted bR was checked in GUVs but not quantified in detail (50). In the present study, we used the same microfluidic setup as for proton pumping in order to assess the permeability of individual GUVs. First, the GUVs, suspended in the electroformation buffer (1 mM Tris·HCl, pH 7.5, containing 100 mM sucrose and 10 μM pyranine), were trapped in the microfluidic chip. Next, nonencapsulated pyranine was flushed away with dye-free buffer, and finally, transmembrane pH gradient was induced by changing the external solution for isosmotic 1 mM MES, pH 6.0, containing ∼100 mM sucrose (Fig. 6*A*, *Inset*). Upon acidification in the microfluidic device, the luminal pH of the different types of GUVs decreased differently (*SI Appendix*, section S17.1 and Fig. S24).

The reported values for proton permeability, which is more accurately denoted as net proton-hydroxyl permeability (80), vary over several orders of magnitude in liposomes (81). This discrepancy partially arises from different setups (pH dye, magnitude of pH gradient, temperature, etc.) and the calculation approaches; for details on the current data analysis, please see *SI Appendix*, section S7.4. The permeability coefficients at the nanometer scale slightly differed from the ones determined at micrometer scale (Fig. 6 *C* and *D* and *SI Appendix*, section S17.4 and Table S5), but the values did not vary by more than an order of magnitude (×5 at most), which is the range of usually reported precision. This variance may be attributed first to the fact that in the bulk assay the integrity of the LUVs is not always guaranteed, and second to the differences in curvature and packing density, which accompany the size variance. This second assumption was supported by the minor difference in passive proton permeability (∼9%) in the case of protein-free polymersomes, in which the structure of the monolayer should be largely preserved, regardless of the size. In the case of bo_3 oxidase-functionalized vesicles, the difference in proton permeability on nano and micro level may also arise from different membrane rearrangement and resealing after detergent removal (in the first case, detergent was removed by gel filtration, while in the second by Bio-Beads). Altogether, with respect to the comparison between different membranes, the trends at different scales were remarkably reproducible.

In the case of protein-free vesicles the proton permeability of polymersomes ($\sim 2 \times 10^{-7}$ cm·s^{-1}) was slightly higher than that of liposomes in GUVs and 3.4× lower in LUVs (*SI Appendix*, section S17.4 and Table S5). In protein-free hybrids, we found different populations of vesicles; some exhibited slightly higher permeability than liposomes and polymersomes, while others exceeded it severalfold, which influenced the mean values correspondingly (Fig. 6*C*). This could obviously not be explained by the superimposition of properties of both membrane constituents, which would result in intermediate values. Instead, we hypothesize that the higher permeability to protons resulted from nanoscale phase separation. At 70 mol% polymer and 30 mol% lipid contents, the hybrid GUVs were exclusively homogeneous under the microscope. We found only a single GUV with observable microdomains in the entire population (500 to 600) of all sample preparations (*SI Appendix*, section 17.2 and Fig. S26) and no phase separation with time was observed (hybrids stayed microscopically homogenous for over a week). Therefore, we speculate that the permeability may be increased because of heterogeneity at the nanoscale, caused by slight size mismatches and different molecular architecture. This would make the membranes more prone to spontaneous pore formation, especially at the phase interfaces. Increased permeability of hybrid membranes in comparison to pure lipid or polymer vesicles was already reported for DOPC/PEO-*b*-PBD blends (76), while nanodomain formation has been recently demonstrated for blends of PDMS-*g*-PEO and DPPC (82), and we further confirmed this in PDMS-*g*-PEO/soy PC hybrids with cryo-TEM. As mentioned in section 3, in larger portion of the hybrid vesicles, we observed nanodomains with lipid bilayer structure and surrounding fuzzy membrane resembling the structure of the polymer membrane (*SI Appendix*, section S18.3 and Fig. S36). Although the hybrids were prepared from 70 mol% polymer and

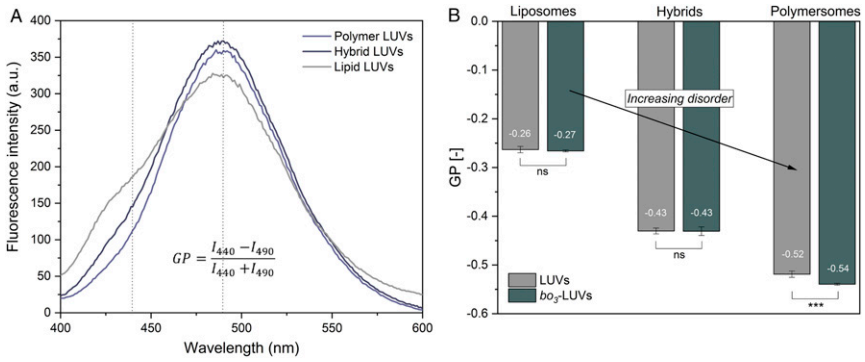

Fig. 5. (*A*) Fluorescence emission spectra of Laurdan in lipid, hybrid, and polymer membranes expressed in arbitrary units (a.u.). (*B*) Generalized polarization (GP) values of protein-free and protein-functionalized LUVs. The black arrow shows the increasing exposure to water indicating increasing membrane disorder. Error bars represent SD from $n = 3$. ns, not significant for $P > 0.05$; ***$P \leq 0.001$.

30 mol% lipid, the composition cannot be perfectly controlled as vesicles are out-of-equilibrium objects, which leads to formation of hybrids with disperse lipid content, and consequently lipid domains (83). Our observations of nanodomains (*SI Appendix*, section 18.3 and Fig. S36) and their size are in agreement with the previous report in PDMS-*g*-PEO/DPPC LUVs [3 to 7 nm, determined via small-angle neutron scattering and FRET (82)]. Importantly, lipid nanodomains in PDMS-*g*-PEO/PC were previously shown to be stable (no budding was observed in LUVs with nanodomains, while the budding occurred in phase-separated GUVs with microdomains) (83). Interestingly, despite the ∼0.9-nm difference in the membrane thickness between the lipid and polymer membranes in the present case, the hybrid membrane had intermediate thickness and therefore no visible size mismatch was detected. A matching thickness between the lipid domains and the surrounding polymer membrane stabilizes the hybrid system by minimizing the line tension (83). Furthermore, the amphiphile mixing was previously shown to be more efficient for graft copolymer than for triblock with the same chemical composition and membrane thickness (PEO-*b*-PDMS-*b*-PEO) (82), giving additional reason for the utilization of PDMS-*g*-PEO for stable hybrid systems.

To further assess the influence of phase separation in hybrids, we deliberately formed microscopically heterogeneous GUVs because we expected that if nanodomains were the cause of increased permeability microdomains should, because of their lower stability, cause similar or even higher proton permeability. To obtain hybrids with microdomains we resorted to the classical electroformation procedure, in which the hybrid amphiphile mixture was deposited on ITO-slides in organic solvent and not in the form of preformed vesicles (*SI Appendix*, section S17.2 and Fig. S27). The permeability of phase-separated hybrid GUVs (with polymer-to-lipid molar ratio of 40:60) was about threefold higher than for homogenous hybrid GUVs ($7.1 \pm 1.9 \times 10^{-6}$ cm·s^{-1}) (*SI Appendix*, section S17.2 and Fig. S28), which confirmed that the proton permeability correlated with the dynamics of phase separation.

The reconstitution of bo_3 oxidase increased the proton permeability of the polymer GUVs, which was supported at the LUV scale (Fig. 6*D*). The scattered data for bo_3 oxidase-functionalized polymersomes and liposomes likely results from the different reconstitution efficiency (GUVs with lower permeability have likely lower protein density). We ascribe the decreased tightness of PDMS-*g*-PEO to the loosening of the polymer structure, as discussed in the case of the increased lateral diffusion (Fig. 4*A*) and membrane disorder (Fig. 5*B*). Permeability coefficients in the order of 10^{-5} cm·s^{-1} at much lower lipid-to-protein weight ratios (40–160:1) were determined in egg PC/PA membranes with reconstituted bR (37). One can anticipate an increase of permeability at higher protein loadings in the present system as well; however, we do not expect that such loadings will be required for efficient bioenergetics.

In contrast to single-component membranes, in hybrids bo_3 oxidase caused an unexpected decrease of permeability for both GUVs and LUVs. To check whether this phenomenon was protein specific, we additionally tested the proton permeability at the LUV scale after insertion of *E. coli* F_1F_o-ATPase and observed the same behavior. The permeability of polymer membranes increased, while the permeability of hybrids decreased (Fig. 6*D* and *SI Appendix*, section S17.4 and Table S5), whereby we note that the type of detergent (sodium cholate [SC] for bo_3 oxidase, octyl glucoside [OG] for F_1F_o-ATPase) used in the reconstitution apparently did not play a role either.

A plausible explanation for the decreased proton permeability of proteohybrid membranes relates to the reorganization of the membrane by protein insertion; lipid molecules rearrange to fill the protein insertion spots and thus counteract the loosening of the polymer chains. To explore the latter hypothesis in greater detail, we next analyzed the partitioning of either lipid (PE-Rho) or polymer dye (PDMS-*g*-PEO-Rho) with respect to bo_3 oxidase-ATTO 514 in hybrid LUVs. In this scenario, the emission of the FRET donor ATTO 514 would be quenched by the FRET acceptor rhodamine when the lipid dye localizes in close proximity to the reconstituted enzyme. Next, the distance between the FRET couple was gradually increased by stepwise dissolution with OG and the ATTO 514 dequenching was monitored. The dequenching profiles differed significantly between the two systems. Most notably, the initial emission intensity of the protein dye was significantly lower with the lipid dye (i.e., quenched), hinting at preferred lipid localization in the vicinity of bo_3 oxidase (Fig. 7*A*, mechanism presented in Fig. 7*C*). Moreover, the addition of OG up to the point of total vesicle solubilization (marked as OG R_{sol}) led to relatively small increase in the emission of ATTO 514 (Fig. 7*A*, steps 1 and 2). This was a further indication of persistent quenching by protein-associated lipids rather than by merely proximal ones (note that the distance between the latter and the enzyme should increase with increasing surfactant resulting in proportional dequenching, which was observed only partially and shortly). Furthermore, while rapid dequenching of the protein dye was observed upon total solubilization to mixed (lipid/polymer/detergent/bo_3) micelles (Fig. 7*A*, "OG R_{sol}"), ATTO 514 was quickly requenched again (Fig. 7*A*, step 4), presumably due to lipid relocation to the protein. Finally, when OG was added at the critical micellar concentration (denoted as "OG CMC"), gradual ATTO 514 dequenching was observed, which was likely a result of PE-Rho leaching to detergent micelles as well as delipidation of bo_3 oxidase. In contrast, the higher initial emission of ATTO 514 with PDMS-*g*-PEO-Rho (i.e., less quenching) indicated larger lateral distance between enzyme and polymer. The dilution of the hybrid membranes resulted in continuous linear dequenching of the polymer dye until the OG R_{sol} (Fig. 7*B*, step 2) and similar steady increase was observed in the micellar phase (Fig. 7*B*, step 3). Both the intensity and dynamics of the FRET experiment with labeled polymer are strong

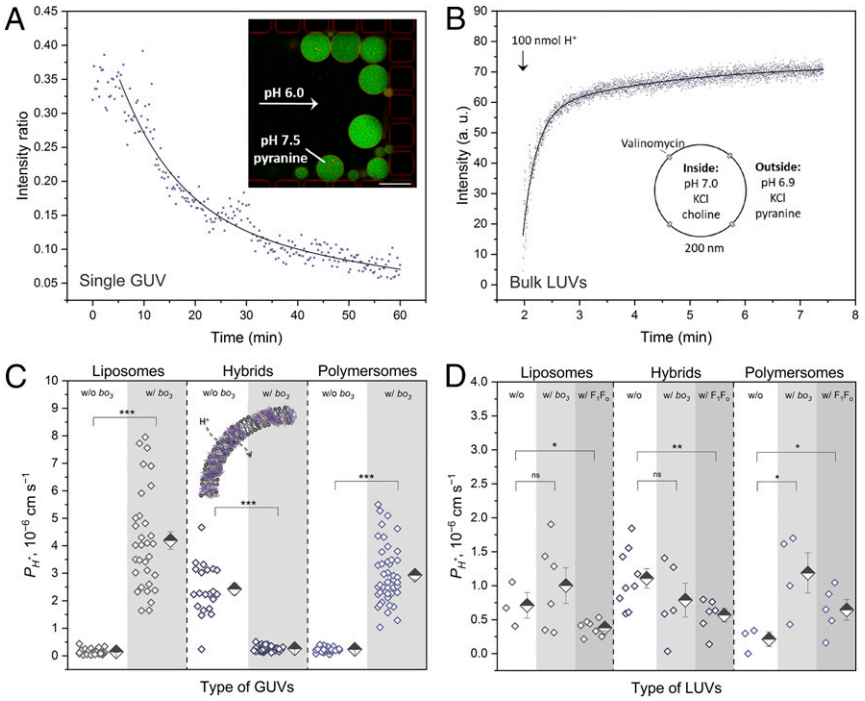

Fig. 6. Passive proton permeability of GUVs and LUVs. (*A*) Fluorescence intensity ratio (excitation, 458/405 nm; emission, 499 to 551 nm) inside a single bo_3-polymer-GUV over time after exchange of external solution with more acidic buffer. Data were fitted with a biexponential decay function ($y = A_1e^{-tk_1} + A_2e^{-tk_2} + y_0$). (Scale bar, 50 μm.) (*B*) Fluorescence intensity (excitation, 450 nm; emission, 508 nm) change of pyranine in external solution of hybrid LUVs after the addition of acid. Data were fitted with biexponential function. (*C*) Permeability coefficients ($P_H{}^+$) of protein-free GUVs (w/o bo_3; white area) and protein-functionalized GUVs (w/ bo_3; gray area). Individual GUV-related data are shown as diamonds. Average values are presented with half-filled diamonds and mean error. (*D*) $P_H{}^+$ of protein-free LUVs (w/o; white area) and protein-functionalized LUVs with bo_3 oxidase (w/ bo_3; gray area) or F_1F_o-ATPase (w/ F_1F_o; dark-gray area). Each diamond represents a separate measurement on LUVs in bulk. Average values are presented with half-filled diamonds and mean error. a.u., arbitrary units; ns, not significant for $P > 0.05$; $*P \leq 0.05$; $**P \leq 0.01$; $***P \leq 0.001$.

indicators of random localization with respect to the enzyme and unrestricted mobility unlike the sustained intimate localization of lipids.

This distinct positioning of the membrane constituents around the enzyme in hybrid membranes may be also the reason behind the preserved activity of bo_3 oxidase over time (section 1). Nevertheless, this arrangement likely results in susceptibility to ROS exposure and lower stability compared to proteopolymersomes (Fig. 1*B*) because the delipidation of its tight surrounding is exposing the protein to aggregation. Furthermore, the entrapment of lipids is in line with their slower diffusion in the polymer membrane after protein insertion (Fig. 4*A*) in contrast to the increased overall membrane fluidity.

It was previously proposed that block copolymer membranes can adjust their thickness to the size of MP, whereby in the case of hydrophobic mismatch between smaller MPs (channels) and thicker PMOXA-*b*-PDMS-*b*-PMOXA membrane (9 to 13 nm) hydrophobic domains around the inserted MPs showed significant compression, explained by the flexibility and low viscosity of PDMS (65). Cryo-TEM revealed that the PDMS-*g*-PEO membrane also compressed in the proximity of the protein (Fig. 8). Meanwhile, the opposite behavior was observed in the hybrid membrane: The thickness around the integrated protein increased (average thickness changed from 4.9 ± 0.17 to 5.3 ± 0.54 nm), which was due to lipid accumulation in the protein surrounding. This rearrangement is most likely the reason behind the resealing of hybrids upon insertion of bo_3 oxidase. In contrast, lipid membranes did not demonstrate adaptation of the thickness to the protein insertion (Fig. 8), which was reflected in increased proton permeability. We consider the apparent sealing of the hybrid membrane by the MP as a beneficial phenomenon, which would sustain pH gradients across the membrane, while making use of the hybrid membrane chemistry.

Conclusions

The replacement and augmentation of natural building blocks with synthetic alternatives may improve some characteristics (e.g., rigidity and tightness, crucial for drug delivery) at the expense of others. Since the scope of bottom-up synthetic biology extends beyond the mere segregation from the environment and aims to reconstitute essential life processes such as selective transport and energy transfer, we also seek for retaining those properties of the interfaces, which are necessary to interact with MPs. PDMS-*g*-PEO appears to accommodate these merits, while providing the virtually unlimited potential of further chemical functionalization. In addition, the polymer appears to increase the shelf life and resistance to ROS.

In this work, we studied the activity of the chemically driven proton pump bo_3 oxidase in different types of compartments and determined its influence on relevant mechanical properties. To this end, we optimized the existing protocols and prepared GUVs (>10 μm) with homogenous protein distribution, whereby we demonstrated that the developed procedures can be used for the reconstitution of other complex MPs. The method resulted in active enzymes with predominantly inward orientation, which in combination with a well-sealed membrane, acidified the lumen of the synthetic compartments. The measurements of proton pumping and passive permeability were done in a microfluidic setup, which enabled better control of experimental conditions and individual tracking. While our main rationale is the establishment of PMF for ATP synthesis, the transmembrane proton gradient should not solely serve F_1F_o-ATPase, but could be also employed for transport, signaling, management of pH-dependent enzymatic reactions, or activation and inhibition of drugs.

The reason for the successful protein insertion and retained activity in PDMS-*g*-PEO is the suitable polymer chemistry, which results in a soft and fluid membrane and allows for unhindered conformational changes and lateral diffusion. The latter has direct implications on other potential scenarios in bottom-up synthetic biology such as the assembly of protein monomers and clusters, fission and fusion for trafficking, as well as equal distribution of membrane constituents upon division. Polymersomes and hybrids have moderately low resistivity to bending deformation ($\kappa = 11.7 \pm 2.1$ and $11.6 \pm 2.4\ k_BT$, respectively) and appear more elastic than lipids. This allows them to undergo deformations and to adjust to the environment for biomedical applications or withstand the mechanical forces exerted in

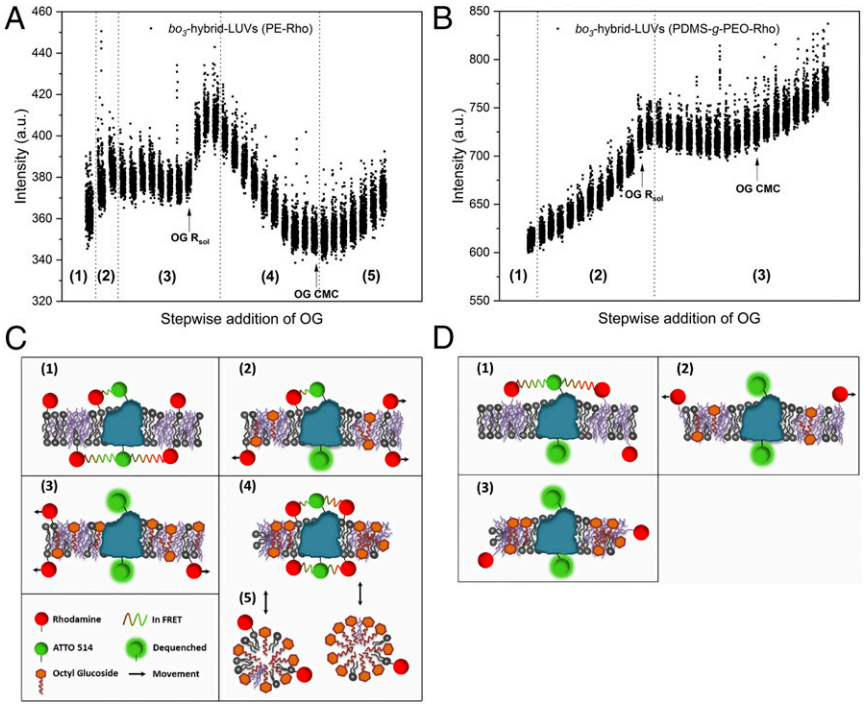

Fig. 7. FRET analysis of lipid and polymer partitioning in the vicinity of bo_3 oxidase, integrated in hybrid membranes. bo_3 oxidase tagged with the FRET donor (ATTO 514) was reconstituted in hybrids containing either fluorescently tagged lipid (PE-Rho), when lipid partitioning was being analyzed (*A*) or fluorescently tagged polymer (PDMS-*g*-PEO-Rho), when polymer partitioning was analyzed (*B*). While in close proximity, rhodamine quenched the emission of ATTO 514, which was being excited. Dequenching was induced by gradual disruption of the membranes via stepwise addition of the detergent octyl glucoside (OG). Two important points are marked on plots (*A* and *B*): the concentration of OG, at which all hybrid LUVs were dissolved to mixed micelles (OG R_{sol}), and the critical micelle concentration of OG (OG CMC). The separate mechanistic steps of the experiment for the partitioning of the lipid or polymer dye are schematically depicted in *C* and *D*, respectively. a.u., arbitrary units.

biotechnology, for instance during agitation. We found that the studied membranes interacted differently with the reconstituted protein. While insertion of bo_3 oxidase in soy PC decreased the fluidity, it exercised the opposite effect on the polymer by loosening its structure. The remarkable finding is that the characteristics of hybrid membranes are not always intermediate between lipid and polymer ones—blending the membrane led to increased permeability and broad distribution, but after proton pump insertion the compartments were surprisingly resealed. By combining biochemical and biophysical approaches, we showed that synthetic building blocks can successfully reproduce the demanding environment required by MPs, offering feasible platform for their integration toward the engineering of an artificial cell. This opens up the possibility of not only mimicking nature but also to the creation of functions that did not exist before.

Methods

Fusion/Electroformation of GUVs. GUVs were prepared from LUVs by modifying the previously published procedure (19). bo_3 oxidase and F_1F_o-ATPase were reconstituted into LUVs via detergent-mediated reconstitution after optimization of our previous protocol (29). For details, see *SI Appendix*.

Preparation of Microfluidic Chips. The wafers were produced by conventional soft lithography methods (84). For chip fabrication, see *SI Appendix*. Each post in the trap has a dimension of 40 by 40 μm, and a height of ∼70 μm; the gap distance between two posts is 5 μm. To prevent the adhesion of GUV to the surface and the resulting rupture, chips were coated with BSA solution.

Oxygen Consumption Measurements. Oxygen consumption measurements were performed with Oxytherm system (Hansatech Instruments). Steady-state activity of reconstituted bo_3 oxidase was determined as described in ref. 29 with slight modifications. For details, see *SI Appendix*.

Vesicles Leakage of CF. Vesicle leakage after exposure to ascorbate and ascorbyl radicals was monitored via the dequenching of encapsulated CF. LUVs were prepared in buffer (100 mM sucrose, 1 mM Tris·HCl, pH 7.5) supplemented with 20 mM CF. To remove the nonencapsulated CF, the vesicle suspension was first run through a Sephadex G-25 column and additionally purified with Nycodenz gradient separation. Fluorescence was monitored at excitation 492 nm and emission 517 nm at constant stirring.

Lateral Diffusion Analysis by FRAP. FRAP experiments were performed using the FRAP booster mode in a Leica TCS SP8 (Wetzlar) microscope with a 63× (1.2 N.A.) water-immersion objective and at 1 Airy unit. Imaging and photobleaching were performed with a 561-nm diode-pumped solid-state laser. Images were acquired with 128 × 128 format at a speed of 1,400 Hz, with no line averaging. In this configuration, the time between frames was 54 ms. Ten prebleach images at low laser intensity were recorded and used as a reference, and then the laser intensity was increased to maximum for another four frames for photobleaching, after which the laser intensity was again decreased to record photobleaching recovery. The nominal (user-defined) photobleaching radius (r_n) was set to 1.5 μm.

Membrane Order Analysis by Laurdan. The emission spectra of Laurdan were monitored in fluorescence spectrophotometer Varian Cary Eclipse (Agilent) at excitation 530 nm and emission 400 to 600 nm. Final lipid/polymer concentration was 200 μM, and final Laurdan concentration was 600 μM.

Passive Proton Permeability.

Passive proton permeability of LUVs. bo_3 oxidase was reconstituted by 0.8% SC in lipid, hybrid, and polymer vesicles (40 mg·mL^{-1}), at final lipid/polymer-to-protein ratios of 9,560:1, 9,550:1, and 9,540:1, respectively. F_1F_o-ATPase was reconstituted at the same ratios but via 2.4% SC in liposomes and 0.4% OG in hybrids and polymersomes. Passive proton permeability of LUVs was determined by adopting a reported protocol (85).

Passive proton permeability of GUVs. The lipid/polymer-to-protein molar ratio in bo_3-GUVs was the same as in bo_3-LUVs. The experiments were performed in microfluidics, as described in main text.

Determination of proton permeability coefficients from intravesicular pyranine fluorescence. The data were fitted with a biexponential curve ($y = A_1e^{-tk_1} + A_2e^{-tk_2} + y_0$), where A is the amplitude of fluorescence signal, k is the first-order rate constant of proton influx, and y_0 is the offset; k_2 was used to calculate the permeability coefficient through the reported relation $P_{H^+} = k(R/3)$ (79), where R was the vesicle radius.

Analysis of bo_3 Oxidase Partitioning in Hybrid Membranes via FRET. bo_3 oxidase labeled with ATTO 514 was reconstituted in hybrid LUVs containing 2 mol% of either lipid dye (PE-Rho) or labeled polymer (PDMS-*g*-PEO-Rho). ATTO 514 fluorescence was monitored at excitation 511 nm and emission 533 nm at constant stirring and 5 °C. OG was added in 30 subsequent 2-μL 10% OG aliquots. After each addition, samples were vortexed for 5 s.

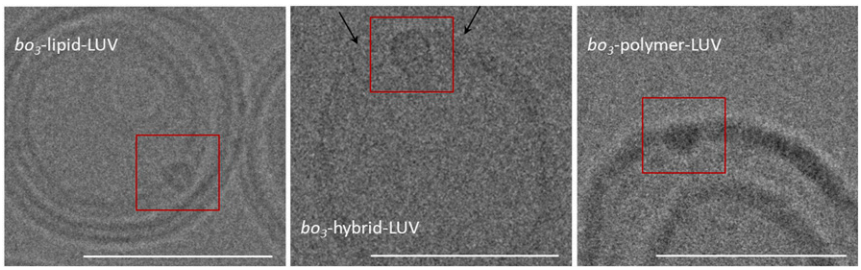

Fig. 8. Cryo-TEM images of lipid, hybrid, and polymer bo_3-LUVs. bo_3 oxidase is marked with a red square. On the *Left* and *Right* image, inward orientation of the cytosolic part (pump in) can be observed; see *SI Appendix*, section S19 and Fig. S41 for bo_3 oxidase dimensions and structure. The black arrows (*Middle* image) show increased membrane thickness around the protein (from 4.9 to ∼7.5 nm) in bo_3-hybrid-LUVs. Lipid bilayer thickness did not change after protein insertion (*SI Appendix*, section S18.1 and Table S6). In bo_3-polymer-LUVs (*Right*), the membrane compressed in the vicinity of the protein (∼4.4 nm) and expanded at further distance (∼6.3 nm), leading to increase in the average thickness (∼5.8 nm). (Scale bar, 50 nm; defocus, approximately −2 μm.)

Cryo-TEM. The vitrification of the samples was carried out using Vitrobot Mark IV System (Thermo Fisher Scientific) and standard Vitrobot Filter Paper (i.e., Ø55/20 mm, Grade 595). For vitrification conditions, see *SI Appendix*. The grid was mounted onto a Thermo FEI Glacios 200 kV autoloader under cryo conditions. Images were acquired using Falcon 3EC direct electron detector in linear mode and a total dose of 50 $e^-/Å^2$.

Data Availability. All relevant data and protocols discussed in the study are available in the main text and *SI Appendix*.

ACKNOWLEDGMENTS. This work is part of the MaxSynBio Consortium, which is jointly funded by the Federal Ministry of Education and Research (Bundesministerium für Bildung und Forschung [BMBF]) of Germany and the Max Planck Society. P.L.K., F.H., and F.L.K. acknowledge funding by Deutsche Forschungsgemeinschaft (Project 391498659, RTG 2467), the BMBF (Zentren für Innovationskompetenz Program; Grant 02Z22HN23), the European Regional Development Funds for Saxony-Anhalt (Grant EFRE: ZS/2016/04/78115), and the Martin Luther University Halle-Wittenberg. We are grateful to Claudia Bednarz for isolation and purification of bo_3 oxidase and F_1F_o-ATPase, to Vasil Georgiev for help with flickering microscopy, and to Andrea Sassoli for help on durability and chemical stability measurements.

1. L. Otrin *et al.*, Artificial organelles for energy regeneration. *Adv. Biosyst.* **3**, 1800323 (2019).
2. J. F. Le Meins, C. Schatz, S. Lecommandoux, O. Sandre, Hybrid polymer/lipid vesicles: State of the art and future perspectives. *Mater. Today* **16**, 397–402 (2013).
3. E. Rideau, R. Dimova, P. Schwille, F. R. Wurm, K. Landfester, Liposomes and polymersomes: A comparative review towards cell mimicking. *Chem. Soc. Rev.* **47**, 8572–8610 (2018).
4. J. S. Lee, J. Feijen, Polymersomes for drug delivery: Design, formation and characterization. *J. Control. Release* **161**, 473–483 (2012).
5. D. E. Discher *et al.*, Emerging applications of polymersomes in delivery: From molecular dynamics to shrinkage of tumors. *Prog. Polym. Sci.* **32**, 838–857 (2007).
6. F. Meng, Z. Zhong, J. Feijen, Stimuli-responsive polymersomes for programmed drug delivery. *Biomacromolecules* **10**, 197–209 (2009).
7. S. Egli *et al.*, Biocompatible functionalization of polymersome surfaces: A new approach to surface immobilization and cell targeting using polymersomes. *J. Am. Chem. Soc.* **133**, 4476–4483 (2011).
8. Y. Lee, J.-B. Chang, H. K. Kim, T. G. Park, Stability studies of biodegradable polymersomes prepared by emulsion solvent evaporation method. *Macromol. Res.* **14**, 359–364 (2006).
9. A. Mata, A. J. Fleischman, S. Roy, Characterization of polydimethylsiloxane (PDMS) properties for biomedical micro/nanosystems. *Biomed. Microdevices* **7**, 281–293 (2005).
10. S. T. Poschenrieder, S. K. Schiebel, K. Castiglione, Stability of polymersomes with focus on their use as nanoreactors. *Eng. Life Sci.* **18**, 101–113 (2018).
11. R. Rodríguez-García *et al.*, Polymersomes: Smart vesicles of tunable rigidity and permeability. *Soft Matter* **7**, 1532–1542 (2011).
12. J. F. Le Meins, O. Sandre, S. Lecommandoux, Recent trends in the tuning of polymersomes' membrane properties. *Eur. Phys. J. E Soft Matter* **34**, 14 (2011).
13. M. Xiao, J. Liu, J. Yang, R. Wang, D. Xie, Biomimetic membrane control of block copolymer vesicles with tunable wall thickness. *Soft Matter* **9**, 2434–2442 (2013).
14. J. Petit *et al.*, A modular approach for multifunctional polymersomes with controlled adhesive properties. *Soft Matter* **14**, 894–900 (2018).
15. B. Kadenbach, Intrinsic and extrinsic uncoupling of oxidative phosphorylation. *Biochim. Biophys. Acta* **1604**, 77–94 (2003).
16. M. P. Murphy, How mitochondria produce reactive oxygen species. *Biochem. J.* **417**, 1–13 (2009).
17. A. W. Girotti, Mechanisms of lipid peroxidation. *J. Free Radic. Biol. Med.* **1**, 87–95 (1985).
18. E. Schnitzer, I. Pinchuk, D. Lichtenberg, Peroxidation of liposomal lipids. *Eur. Biophys. J.* **36**, 499–515 (2007).
19. P. Girard *et al.*, A new method for the reconstitution of membrane proteins into giant unilamellar vesicles. *Biophys. J.* **87**, 419–429 (2004).
20. E. Altamura *et al.*, Highly oriented photosynthetic reaction centers generate a proton gradient in synthetic protocells. *Proc. Natl. Acad. Sci. U.S.A.* **114**, 3837–3842 (2017).
21. O. Biner, T. Schick, Y. Müller, C. von Ballmoos, Delivery of membrane proteins into small and giant unilamellar vesicles by charge-mediated fusion. *FEBS Lett.* **590**, 2051–2062 (2016).
22. V. G. Almendro-Vedia *et al.*, Nonequilibrium fluctuations of lipid membranes by the rotating motor protein F_1F_0-ATP synthase. *Proc. Natl. Acad. Sci. U.S.A.* **114**, 11291–11296 (2017).
23. M. Garni, S. Thamboo, C. A. Schoenenberger, C. G. Palivan, Biopores/membrane proteins in synthetic polymer membranes. *Biochim. Biophys. Acta Biomembr.* **1859**, 619–638 (2017).
24. S. Khan, M. Li, S. P. Muench, L. J. Jeuken, P. A. Beales, Durable proteo-hybrid vesicles for the extended functional lifetime of membrane proteins in bionanotechnology. *Chem. Commun. (Camb.)* **52**, 11020–11023 (2016).
25. R. Dimova, U. Seifert, B. Pouligny, S. Förster, H.-G. Döbereiner, Hyperviscous diblock copolymer vesicles. *Eur. Phys. J. E* **7**, 241–250 (2002).
26. R. Goers *et al.*, Optimized reconstitution of membrane proteins into synthetic membranes. *Commun. Chem.* **1**, 35 (2018).
27. A. Graff *et al.*, Amphiphilic copolymer membranes promote NADH:ubiquinone oxidoreductase activity: Towards an electron-transfer nanodevice. *Macromol. Chem. Phys.* **211**, 229–238 (2010).
28. H. J. Choi, C. D. Montemagno, Artificial organelle: ATP synthesis from cellular mimetic polymersomes. *Nano Lett.* **5**, 2538–2542 (2005).
29. L. Otrin *et al.*, Toward artificial mitochondrion: Mimicking oxidative phosphorylation in polymer and hybrid membranes. *Nano Lett.* **17**, 6816–6821 (2017).
30. A. Musatov *et al.*, Detergent-solubilized *Escherichia coli* cytochrome bo_3 ubiquinol oxidase: A monomeric, not a dimeric complex. *FEBS Lett.* **457**, 153–156 (1999).
31. M. M. Pereira, M. Santana, M. Teixeira, A novel scenario for the evolution of haem-copper oxygen reductases. *Biochim. Biophys. Acta* **1505**, 185–208 (2001).
32. J.-B. Manneville, P. Bassereau, D. Lévy, J. Prost, "Magnification of shape fluctuations of active giant unilamellar vesicles" in *Giant Vesicles: Perspectives in Supramolecular Chemistry*, P. L. Luisi, P. Walde, Eds. (Wiley, 1999), vol. 6, pp. 351–360.
33. P. Girard, J. Prost, P. Bassereau, Passive or active fluctuations in membranes containing proteins. *Phys. Rev. Lett.* **94**, 088102 (2005).
34. H. Bouvrais, F. Cornelius, J. H. Ipsen, O. G. Mouritsen, Intrinsic reaction-cycle time scale of Na^+,K^+-ATPase manifests itself in the lipid-protein interactions of nonequilibrium membranes. *Proc. Natl. Acad. Sci. U.S.A.* **109**, 18442–18446 (2012).
35. J. E. Goose, M. S. Sansom, Reduced lateral mobility of lipids and proteins in crowded membranes. *PLOS Comput. Biol.* **9**, e1003033 (2013).
36. S. Ramadurai *et al.*, Lateral diffusion of membrane proteins. *J. Am. Chem. Soc.* **131**, 12650–12656 (2009).
37. M. Seigneuret, J. L. Rigaud, Analysis of passive and light-driven ion movements in large bacteriorhodopsin liposomes reconstituted by reverse-phase evaporation. 1. Factors governing the passive proton permeability of the membrane. *Biochemistry* **25**, 6716–6722 (1986).
38. N. Yandrapalli, T. Robinson, Ultra-high capacity microfluidic trapping of giant vesicles for high-throughput membrane studies. *Lab Chip* **19**, 626–633 (2019).
39. L. S. Khailova, V. I. Dedukhova, E. N. Mokhova, Cations SkQ1 and MitoQ accumulated in mitochondria delay opening of ascorbate/$FeSO_4$-induced nonspecific pore in the inner mitochondrial membrane. *Biochemistry (Mosc.)* **73**, 1121–1124 (2008).
40. S. R. Schaffazick, A. R. Pohlmann, C. A. S. de Cordova, T. B. Creczynski-Pasa, S. S. Guterres, Protective properties of melatonin-loaded nanoparticles against lipid peroxidation. *Int. J. Pharm.* **289**, 209–213 (2005).
41. M. Li *et al.*, Single enzyme experiments reveal a long-lifetime proton leak state in a heme-copper oxidase. *J. Am. Chem. Soc.* **137**, 16055–16063 (2015).
42. R. Seneviratne *et al.*, A reconstitution method for integral membrane proteins in hybrid lipid-polymer vesicles for enhanced functional durability. *Methods* **147**, 142–149 (2018).

43. B. L. Mui, P. R. Cullis, E. A. Evans, T. D. Madden, Osmotic properties of large unilamellar vesicles prepared by extrusion. *Biophys. J.* **64**, 443–453 (1993).
44. R. Dimova, C. Marques, *The Giant Vesicle Book* (CRC Press, ed. 1, 2019).
45. M. I. Angelova, S. Soléau, P. Méléard, F. Faucon, P. Bothorel, *Preparation of Giant Vesicles by External AC Electric Fields. Kinetics and Applications* (Steinkopff, 1992), pp. 127–131.
46. S. Pautot, B. J. Frisken, D. A. Weitz, Production of unilamellar vesicles using an inverted emulsion. *Langmuir* **19**, 2870–2879 (2003).
47. J. Sjöholm *et al*., The lateral distance between a proton pump and ATP synthase determines the ATP-synthesis rate. *Sci. Rep.* **7**, 2926 (2017).
48. B. Mattei, R. B. Lira, K. R. Perez, K. A. Riske, Membrane permeabilization induced by Triton X-100: The role of membrane phase state and edge tension. *Chem. Phys. Lipids* **202**, 28–37 (2017).
49. M. Chemin, P.-M. Brun, S. Lecommandoux, O. Sandre, J.-F. Le Meins, Hybrid polymer/lipid vesicles: Fine control of the lipid and polymer distribution in the binary membrane. *Soft Matter* **8**, 2867–2874 (2012).
50. M. Dezi, A. Di Cicco, P. Bassereau, D. Lévy, Detergent-mediated incorporation of transmembrane proteins in giant unilamellar vesicles with controlled physiological contents. *Proc. Natl. Acad. Sci. U.S.A.* **110**, 7276–7281 (2013).
51. N. R. Clement, J. M. Gould, Pyranine (8-hydroxy-1,3,6-pyrenetrisulfonate) as a probe of internal aqueous hydrogen ion concentration in phospholipid vesicles. *Biochemistry* **20**, 1534–1538 (1981).
52. S. Gupte *et al*., Relationship between lateral diffusion, collision frequency, and electron transfer of mitochondrial inner membrane oxidation-reduction components. *Proc. Natl. Acad. Sci. U.S.A.* **81**, 2606–2610 (1984).
53. M. Seigneuret, J. L. Rigaud, Analysis of passive and light-driven ion movements in large bacteriorhodopsin liposomes reconstituted by reverse-phase evaporation. 2. Influence of passive permeability and back-pressure effects upon light-induced proton uptake. *Biochemistry* **25**, 6723–6730 (1986).
54. C. von Ballmoos, O. Biner, T. Nilsson, P. Brzezinski, Mimicking respiratory phosphorylation using purified enzymes. *Biochim. Biophys. Acta* **1857**, 321–331 (2016).
55. P. Méléard *et al*., Mechanical properties of model membranes studied from shape transformations of giant vesicles. *Biochimie* **80**, 401–413 (1998).
56. R. Dimova, Recent developments in the field of bending rigidity measurements on membranes. *Adv. Colloid Interface Sci.* **208**, 225–234 (2014).
57. P. Méléard, T. Pott, H. Bouvrais, J. H. Ipsen, Advantages of statistical analysis of giant vesicle flickering for bending elasticity measurements. *Eur. Phys. J. E Soft Matter* **34**, 116 (2011).
58. R. S. Gracia, N. Bezlyepkina, R. L. Knorr, R. Lipowsky, R. Dimova, Effect of cholesterol on the rigidity of saturated and unsaturated membranes: Fluctuation and electrodeformation analysis of giant vesicles. *Soft Matter* **6**, 1472–1482 (2010).
59. M. Karimi *et al*., Asymmetric ionic conditions generate large membrane curvatures. *Nano Lett.* **18**, 7816–7821 (2018).
60. M. D. El Alaoui Faris *et al*., Membrane tension lowering induced by protein activity. *Phys. Rev. Lett.* **102**, 038102 (2009).
61. J.-B. Manneville, P. Bassereau, D. Lévy, J. Prost, Activity of transmembrane proteins induces magnification of shape fluctuations of lipid membranes. *Phys. Rev. Lett.* **82**, 4356–4359 (1999).
62. P. Bassereau, B. Sorre, A. Lévy, Bending lipid membranes: Experiments after W. Helfrich's model. *Adv. Colloid Interface Sci.* **208**, 47–57 (2014).
63. H. M. Berman *et al*., The Protein Data Bank. *Nucleic Acids Res.* **28**, 235–242 (2000).
64. J. B. Manneville, P. Bassereau, S. Ramaswamy, J. Prost, Active membrane fluctuations studied by micropipet aspiration. *Phys. Rev. E Stat. Nonlin. Soft Matter Phys.* **64**, 021908 (2001).
65. F. Itel, A. Najer, C. G. Palivan, W. Meier, Dynamics of membrane proteins within synthetic polymer membranes with large hydrophobic mismatch. *Nano Lett.* **15**, 3871–3878 (2015).
66. A. G. Lee, How lipids affect the activities of integral membrane proteins. *Biochim. Biophys. Acta* **1666**, 62–87 (2004).
67. J. Nam, P. A. Beales, T. K. Vanderlick, Giant phospholipid/block copolymer hybrid vesicles: Mixing behavior and domain formation. *Langmuir* **27**, 1–6 (2011).
68. F. Heinemann, V. Betaneli, F. A. Thomas, P. Schwille, Quantifying lipid diffusion by fluorescence correlation spectroscopy: A critical treatise. *Langmuir* **28**, 13395–13404 (2012).
69. T. P. T. Dao *et al*., The combination of block copolymers and phospholipids to form giant hybrid unilamellar vesicles (GHUVs) does not systematically lead to "intermediate" membrane properties. *Soft Matter* **14**, 6476–6484 (2018).
70. J. C.-M. Lee, M. Santore, F. S. Bates, D. E. Discher, From membranes to melts, rouse to reptation: Diffusion in polymersome versus lipid bilayers. *Macromolecules* **35**, 323–326 (2002).
71. F. Itel *et al*., Molecular organization and dynamics in polymersome membranes: A lateral diffusion study. *Macromolecules* **47**, 7588–7596 (2014).
72. D. Okuno, R. Iino, H. Noji, Rotation and structure of FoF1-ATP synthase. *J. Biochem.* **149**, 655–664 (2011).
73. L. A. Bagatolli, To see or not to see: Lateral organization of biological membranes and fluorescence microscopy. *Biochim. Biophys. Acta* **1758**, 1541–1556 (2006).
74. H.-J. Kaiser *et al*., Order of lipid phases in model and plasma membranes. *Proc. Natl. Acad. Sci. U.S.A.* **106**, 16645–16650 (2009).
75. A. Wiedenmann, P. Dimroth, C. von Ballmoos, Deltapsi and DeltapH are equivalent driving forces for proton transport through isolated F_0 complexes of ATP synthases. *Biochim. Biophys. Acta* **1777**, 1301–1310 (2008).
76. W. F. Paxton, P. T. McAninch, K. E. Achyuthan, S. H. R. Shin, H. L. Monteith, Monitoring and modulating ion traffic in hybrid lipid/polymer vesicles. *Colloids Surf. B Biointerfaces* **159**, 268–276 (2017).
77. M. G. Elferink, J. G. de Wit, A. J. Driessen, W. N. Konings, Stability and proton-permeability of liposomes composed of archaeal tetraether lipids. *Biochim. Biophys. Acta* **1193**, 247–254 (1994).
78. R. H. Gensure, M. L. Zeidel, W. G. Hill, Lipid raft components cholesterol and sphingomyelin increase H^+/OH^- permeability of phosphatidylcholine membranes. *Biochem. J.* **398**, 485–495 (2006).
79. C. L. Kuyper, J. S. Kuo, S. A. Mutch, D. T. Chiu, Proton permeation into single vesicles occurs via a sequential two-step mechanism and is heterogeneous. *J. Am. Chem. Soc.* **128**, 3233–3240 (2006).
80. J. W. D. D. W. Nichols, D. W. Deamer, Net proton-hydroxyl permeability of large unilamellar liposomes measured by an acid-base titration technique. *Proc. Natl. Acad. Sci. U.S.A.* **77**, 2038–2042 (1980).
81. D. W. Deamer, J. W. Nichols, Proton-hydroxide permeability of liposomes. *Proc. Natl. Acad. Sci. U.S.A.* **80**, 165–168 (1983).
82. T. P. T. Dao *et al*., Mixing block copolymers with phospholipids at the nanoscale: From hybrid polymer/lipid wormlike micelles to vesicles presenting lipid nanodomains. *Langmuir* **33**, 1705–1715 (2017).
83. T. P. T. Dao *et al*., Phase separation and nanodomain formation in hybrid polymer/lipid vesicles. *ACS Macro Lett.* **4**, 182–186 (2015).
84. S. Deshpande, Y. Caspi, A. E. C. Meijering, C. Dekker, Octanol-assisted liposome assembly on chip. *Nat. Commun.* **7**, 10447 (2016).
85. S. V. Albers, W. N. Konings, A. J. M. Driessen, Membranes of thermophiles and other extremophiles. *J. Microbiol. Methods* **35**, 161–171 (2006).